

ATMOSPHERIC PATTERN CLASSIFICATION USING NEURAL NETWORK

NARAYAN CHANDRA DEB

Electronics and Communication Sciences Unit
Indian Statistical Institute 203, B T Road, Kolkata, India
email:narayan@isical.ac.in, narayandeb@gmail.com

ABSTRACT. The thermal structure of the atmosphere varies with the characteristics of the atmosphere. The remote sensing tool SODAR (SOund Detection And Ranging) system is capable of capturing various atmospheric thermal structure patterns that need proper identification and analysis. The analysis of different patterns provides significant input to the understanding of atmospheric processes of the Planetary Boundary Layer (PBL). The expert in this domain only can identify properly different types of atmospheric patterns. The manual identification is a tedious task. Therefore the main objective of this work is to develop an automatic atmospheric pattern classifier using multi-layer perception (MLP) neural network in order to avoid the manual identification. Proposed neural network based SODAR structure classification method is developed based on significant features of the backscattered signals captured by the SODAR system. Plot of backscattered signals intensities in the height and time scale generate image that representing different thermal structure patterns of the atmosphere due to various dynamics of the PBL. Total 600 data sets are selected from the known structure pattern to design the classifier. Acceptable training and test results are being presented in this paper.

Keywords - neural networks, SODAR, PBL, multi-layer perception.

1. INTRODUCTION

Automatic recognition of various atmospheric structure patterns of the Planetary Boundary Layers (PBL) in the lower part of atmosphere are of great importance to the scientific community all over the globe. Many researchers are engaged towards the development for state of the art technology using various computational tools. As we know that the lower part of the atmosphere is influenced by the earth's underlying surface, therefore the studies of wind flow, thermal structure and characteristics of the Atmospheric Boundary Layer (ABL) are very important for the development of various prediction systems. Hence, it is necessary to understand and characterize the dynamics of the ABL. The remote sensing tool SODAR system has been deployed over the past few decades to probe the ABL. Various published works (McAllister et al., 1969; Cronenwett et al., 1972; Beran et al., 1973; Frisch et al., 1974; Wendler et al., 1983; Asimakopoulous et al., 1976) proved the utility of this remote sensing technology for ABL study. With these objectives in mind, a monostatic SODAR was designed, developed and installed at the Indian Antarctic station, Maitri (70.80°S , 11.7°E) and operated it in the harsh polar climatic conditions for over 6 years (1991 to 1997). The design and development (Deb et al., 1995) of this dedicated equipment and its utilization to understand various intricacies of the polar environment are being highlighted in the subsequent sections. The physical process and the development of different observed structure patterns are described by

Deb et al. (2010, 2011). The SODAR system generated huge volume of data which was collected from Antarctica and interpretation of those data was a challenging task to us. Manual interpretation is a tedious job and obviously prone to errors. This motivated us to develop a SODAR structure recognition method. Different studies (Kalogiros et al. 1995, Mukherjee et al. 2002, Choudhury and Mitra 2004) have discussed the classification of SODAR structures. Two computational approaches are used: one based on traditional pattern recognition techniques and the other one is neurocomputing approach. Chaudhuri et al. (1992) developed the SODAR structure classification algorithm based on shape parameters of atmospheric boundary layer (ABL) patterns being represented in the SODAR pattern and the background. Kalogiros et al. (1995) proposed a SODAR structure classification algorithm using image processing and pattern recognition techniques. This algorithm is designed using the features computed from SODAR data of the atmospheric boundary layers. Later Mukherjee et al. (2002) enhanced the SODAR structure classification method by using fractal features. Mukherjee et al. (1999) proposed a SODAR structure identification method using a neural network only for convective and inversion structures. Choudhury and Mitra (2004) proposed a SODAR structure classification model using a neural network for six different structures. Deb et al. (2010, 2011) already developed two atmospheric structures classification methods: one is neural network based offline method which is capable to classify 10 types of atmospheric structures using 39 computed features from SODAR data and 15 meteorological features. Other one is graph matching method by using features from frequency domain analysis of SODAR data to classify eight distinct classes of atmospheric structures. In the present paper we propose a SODAR structure recognition method using multi-layer perceptron where only nine features from the time domain data analysis are being used to classify eight distinct structure patterns more accurately. An on-line implementation of SODAR structure data classification method is also described in this paper.

2. BASIC WORKING PRINCIPLE OF THE SODAR SYSTEM

The SODAR system utilizes sound waves instead of radio waves as employed by the RADAR (RADio Detection And Ranging). The system transmits high power (100 watt, electrical) short pulse (50ms) sound waves of certain frequency (1000-1500 Hz) into the atmosphere by means of specialized antennas.

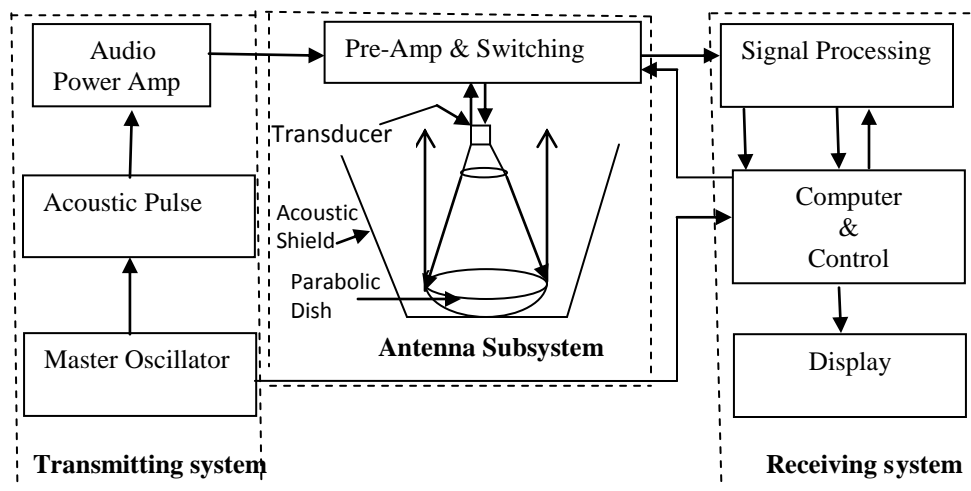


Figure 1: Block diagram of SODAR

These pulses are then interact with the atmospheric turbulence structures (the irregular fluctuations of small-scale horizontal and vertical wind currents resulting from both mechanical or thermal forces) to scatter their energy in all directions. Some of the acoustic energy is always reflected back towards the sound source. That backscattered energy (atmospheric echo) is measured by the SODAR system up to a vertical height range of one kilometer. Both the intensity and frequency of the return signal are monitored to estimate wind components, radial velocity and above all the thermal structure of the atmosphere. A schematic diagram of SODAR system is shown in Fig. 1. It consists of three main subsystems such as transmitting subsystem, antenna subsystem, and receiving subsystem.

3. SODAR SYSTEM OPERATION IN ANTARCTICA

One monostatic SODAR system was operated at Indian Antarctic base in Antarctica for six years. Topography, installation of the system and data collection are discussed in subsequent sections.

3.1 Topography of the Operating Site. Maitri (70.7°S , 11.7°E), is situated on rocky terrain over the Schirmachar region of East Antarctica at 120 m above sea level. Figure 2 depicts map of Antarctica (Koul, 1995). In the map, Schirmachar region seems to be located on the periphery of the continent touching the ocean, but in reality, shelf extending up to above 70 km towards north sector of the Schirmachar region separates the oasis from being close to the open ocean in Antarctica. The oasis extends from east to west tending to low lying 'moraine' of the glacier and it is basically rocky, barren with hilly undulations. It lies between the latitude $70^{\circ} 44' 33'' \text{S}$ to $70^{\circ} 44' 30'' \text{S}$ and longitude $11^{\circ} 22' 40'' \text{E}$ to $11^{\circ} 54' 00'' \text{E}$. The size of the area is about 32.5sq. km having low-lying hills (50 to 200m high) interspersed with small glacial lakes ranging in size from 0.02 to 0.15 km². In the Schirmachar region, the intense sunshine during the summer period results in well-defined convective activity.

3.2 SODAR System Installation and Data Collection. Computer based a monostatic (single antenna acts for both to transmit and to receive) SODAR system was designed, developed and installed at Indian research base 'Maitri' in Antarctica in 1991 (Deb *et al.* 1995) during 11th Indian Scientific Expedition to Antarctic (ISEA) under the Indian Antarctic research program. Author had been to Antarctica and stayed 14 months there to run the SODAR system. Figure 3 depicts antenna system and instrument in the laboratory hut at Maitri, Antarctica. The system could run automatically round the clock basis.

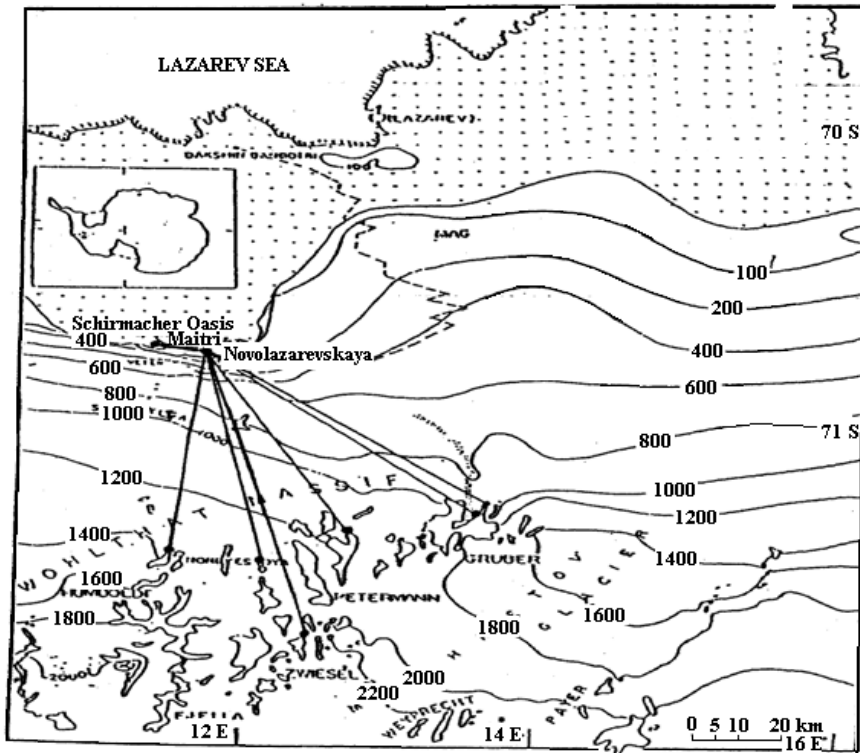


Figure 2: Indian station 'Maitri' located on Schirmachar oasis near the ice shelf.



Figure 3: SODAR antenna system and instrument at Maitri, Antarctica.

During transmission, a high power (15 watt acoustic) pulse was transmitted at every 20-second interval. After sending 50 millisecond width of 1800 Hz acoustic pulse, system sets to receive the backscattered echo and remains active for the next 6 seconds. Thus the maximum height up to which the sound wave traces is the height travelled by the sound pulse in $6/2 = 3$ seconds. This is roughly 1km (taking the velocity of sound in air being 330 metre/second and that the sound pulses are transmitted vertically). In receiving mode it detected backscattered signals for 6 seconds to scan 1kilometre height range. For the rest 14 seconds, it was an idle time for the equipment. The data constitutes from the backscattered signal strength received at the SODAR system from varying heights of the atmosphere as calculated from their time of return. Signals from greater height will presumably take a greater time to return. The return signal after necessary processing

were digitized (400 value in 6 second every 20 second intervals) and stored in permanent storage device round the clock basis automatically using a special format (scattering strength of signals from different heights) along with the stamp of station, date and time.

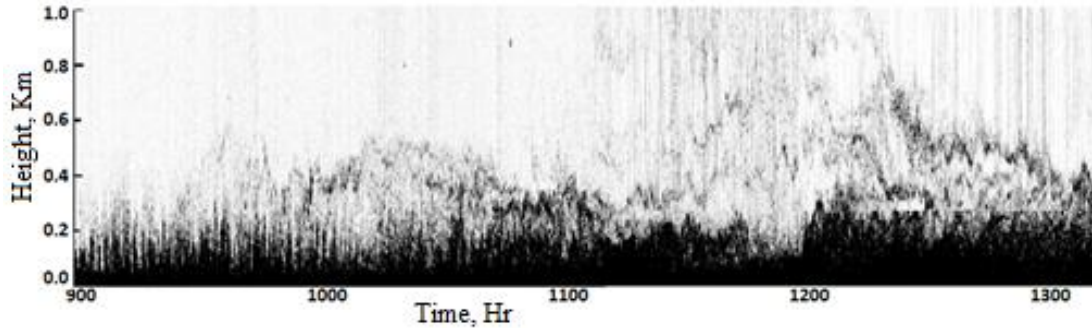


Figure 4: Structure pattern plotted from SODAR data for January 27, 1996

Then height, time and intensity of signals are plotted to generate image to view the structure patterns. For each SODAR scan 400 intensity values are first converted its equivalent gray value one by one using the expression $\left(\frac{\text{value}}{4096}\right) \times 255$, where 4096 is the highest value of data, then plotted on the screen to obtain the image where 'X' axis is treated as time scale and the 'Y' axis is treated as height scale as shown in Fig. 4. Various types of SODAR structures are observed during (1991 – 1997) the operation of the system. All these data were used for the Antarctic boundary layer study (Naithani et al., 1994, 1995; Deb et al., 1999, 2001; Dutta et al., 1999; Gajananda et al., 2004; Kumar et al., 2007). The structures are identified in different classes by expert meteorologist. Ten types of structure patterns are observed during operation. Percentage occurrences of all the structure patterns are shown in Fig. 5 and class names are tabulated in Table 1.

Table 1: Observed structure patterns and their class descriptions.

Class No.	Description of SODAR structure pattern
1	Inversion with force convection (IFC)
2	Inversion with tall spike (IT)
3	Inversion with single elevated layer (IL1)
4	Inversion with two elevated layer (IL2)
5	Inversion with more than two layer (ILM)
6	Inversion with wave motion (IW)
7	Inversion with one or two elevated layer in wave motion (IWE)
8	Inversion with more than two elevated layer in wave motion (IWM)
9	Inversion with small spike (IS)
10	Convection or thermal plumes (TP)

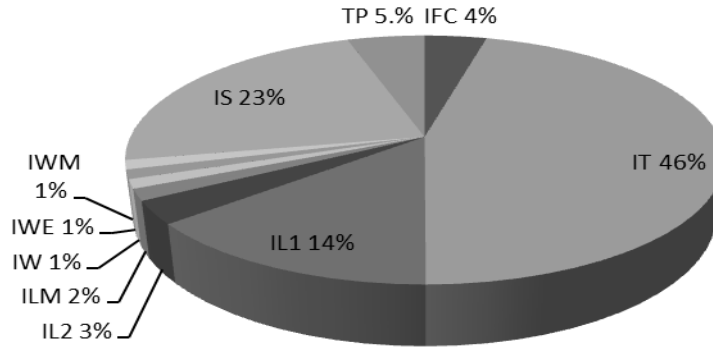


Figure 5: Percentage occurrences of different structures as observed at Maitri, Antarctica, during 1995-1997.

For this classification work we have considered only the class that appeared at site for at least 2% or more occasions during observations recorded over a complete year. Fig. 5 shows three classes (IW, IWE, IWM) whose percentage occurrence $< 2\%$ and these three classes are considered as a single class IEW on the basis of similar wave motion characteristics. In this work, eight different structure patterns were selected using human expert knowledge in this field. All these structure patterns were generated from the data obtained by the system operated at Indian Antarctic base “Maitri” during 1995-1997. The images of selected structure pattern classes are depicted in Figs. 6(a) – (h) and significant property and relation with atmospheric process for the formation of all these classes are described subsequently. From the graphical observation we have extracted each segment (block of 400×180) for each class of structure from continuous data. Data are represented as 3D image where X represents time, Y represents height, and intensity variation is third dimension. From this pictorial representation of data various selected structures were marked into different classes (Table 2) with the expert knowledge.

Table 2: Selected SODAR structure pattern classes.

Class No.	Description of SODAR structure pattern
1	Inversion with force convection (IFC), Fig. 6(a)
2	Inversion with tall spike (IT), Fig. 6(b)
3	Inversion with single elevated layer (IL1), Fig. 6(c)
4	Inversion with two elevated layer (IL2), Fig. 6(d)
5	Inversion with more than two layer (ILM), Fig. 6(e)
6	Inversion with elevated layer in wave motion (IEW), Fig. 6(f)
7	Inversion with small spike (IS), Fig. 6(g)
8	Convection or thermal plumes (TP), Fig. 6(h)

3.3 Description of Atmospheric Pattern for Different Classes. All these eight selected structure classes are representing a different thermodynamic state of the lower ABL. From Table 2 it is evident that there are two main categories of structure inversion and convection. Again among the inversion classes, there are 7 sub-classes.

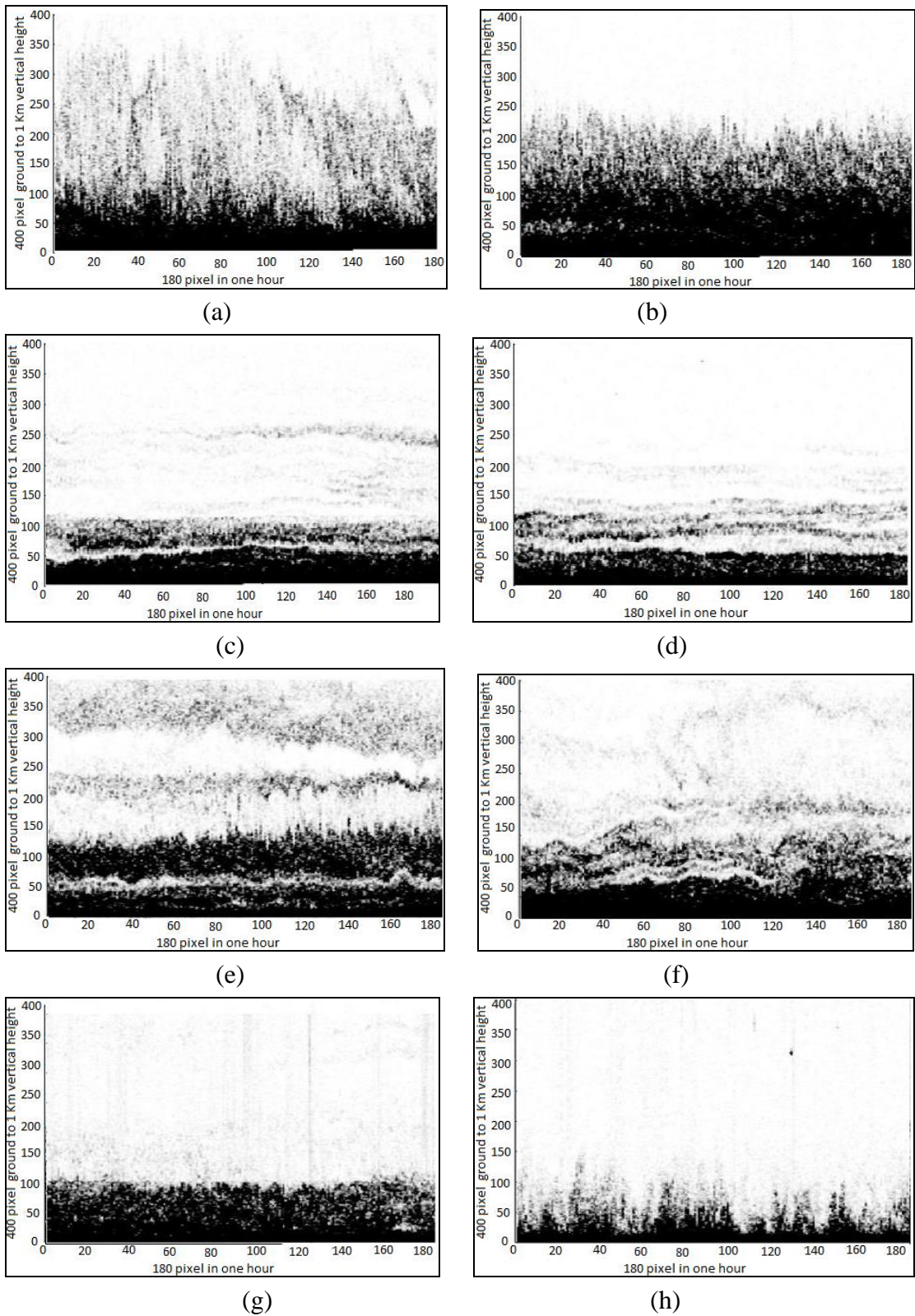


Figure 6: Eight different classes of SODAR structure (a) IFC, (b) IT, (c) IL1, (d) IL2, (e) ILM, (f) IEW, (g) IS, and (h) TP.

Atmospheric inversion is a phenomenon where temperature increases with increasing height in the atmosphere instead of the usual inverse relation of temperature with altitude. Under certain conditions, the normal vertical temperature gradient is inverted such that the air is colder near the surface of the earth. This can occur when, a warmer, less dense air mass moves over a cooler, dense air mass. So temperature inversion occurs when the air temperature increases with height above the earth's surface. The different types of inversion occur in the vicinity of warm fronts. An inversion is also produced whenever radiation from the surface of the earth exceeds the amount of radiation received from the sun, which commonly occurs at night, or during the winter when the angle of the sun is very low in the sky. In Antarctica, about 95% of the time, inversions were recorded. Some inversions were weak and dissipated quickly while others hang for several days depending on the weather pattern. It was possible to record these inversions only for winds below 12 mtr/s and beyond this wind speed, noise masks all the received signals. We are discussing briefly about all types of inversion structures.

IFC (Inversion with Force Convection): Convection or advection is the movement of fluids, atmospheric air packets in this case. In case of forced convection, the fluid movement is not usually affiliated to natural forces like buoyancy. Sometimes, in high wind conditions, the temperature inversion layer may be associated with force convection, as shown in Fig 6.(a).

IT (Inversion with Tall spike): The inversion layer shows tall spike like structures. Under moderately high wind conditions, the temperature inversion layers formed are associated with tall spikes, as seen on the top of the layer. Formation of a temperature inversion layer with tall spikes is shown in Fig 6.(b).

IL1 (Inversion with *single* elevated Layer): If there is an elevated part of the atmosphere on the top of the surface based inversion layer, then IL1 is said to occur. At times an inversion layer may be associated with single elevated layer, as shown in Fig 6(c).

IL2 (Inversion with *two* elevated Layer): The temperature inversion layer may be associated with two elevated layers, as observed in Fig. 6(d). This condition is favourable to form two elevated stable inversion layers.

ILM (Inversion with *more* than two elevated Layer): Sometimes, under very light wind conditions, the temperature inversion layer may be associated with more than two elevated layers, as observed in Fig. 6(e).

IEW (Inversion with Elevated layer in Wave motion): Inversion with wave like structured layer form under light wind conditions and this temperature inversion layer may be associated with wave motion, as observed in Fig. 6(f).

IS (Inversion with Small spike): During low wind, clam condition and absence of solar energy temperature inversion layer with small spike is generally developed which is shown in Fig. 6(g).

TP (Thermal Plumes): Thermal Plumes or Convection happens because warm air is less dense than the cold air around it, so it is lighter and rises or goes up in the atmosphere.

Evidence of convection happening is seen when the sky is clear without clouds. There is a constant balancing act going on all the time in our atmosphere as moist, warm air goes upward and cooler, denser air moves down. This result in the formation of structures called thermal plumes. Figure 6(h) describes the formation of typical convective boundary layer with thermal plumes. Plume structures were seen to appear on cloudless, clear sunny weather. This class represents an unstable atmospheric condition, in which the transfer of heat, momentum, and energy from the surface level to the higher level and vice-versa takes place. This layer brings a drastic change in the thermodynamic state of the ABL.

4. DATA PREPARATION AND FEATURE EXTRACTION

Selected data block of one hour contains (180×400) pixel value is the basic information for each class. From this selected block of data further 15 sets each of (12×400) 4 minutes data are taken for this classification work and referred as segment. From each segment different features were extracted to design and test the classifier. The steps involved to extract required features from the SODAR data and subsequent classification scheme are given below:

- Step 1: Forming the time diagram from data (pixel information)
- Step 2: Plot of averaging/mean
- Step 3: Smoothing of average using spline
- Step 4: Calculating peaks, valleys using gradient
- Step 5: Calculation of envelop peak, and notch
- Step 6: Calculation of envelop area, integral value
- Step 7: Formation of histograms
- Step 8: Calculation of moments

4.1 Formation of Time Diagram from the Data (Pixel Information). A group of 15 data sets (12×400) from one hour data block (180×400) are taken to generate time diagrams. For each set the 400×12 data points are plotted. Thus the abscissa has a size of 1 to 400 whereas the ordinate ranges from 0 to maximum amplitude of 4095. Such 12 clusters are plotted one over the other in a singular graph giving us the time diagram for eight classes as shown in Fig. 7.

4.2 Calculation of Average or Mean. For each of the 15 groups for an individual data set, an averaging is done for the created time diagrams. Thus the abscissa of the plot for the mean still has 400 points whereas along the ordinate is plotted the average value formed from the 12 clusters of values at each of the 400 data points. As a result this average plot contains the mean value of data recorded over a time of 4 minutes.

4.3 Smoothing of average plot. The average plot thus formed is more or less zigzag in nature. In order to process the mean data, such an abrupt plot would not have sufficient.

Therefore in order to get a smoother version of the plot we resort to cubic spline method. A smoother plot is thus obtained allowing us to proceed with finding the gradient of the above mentioned plot. This has been done by selecting around 25-30 data points at regular intervals from the mean plot and then plotting them by interpolating the abscissa back to a domain of 400 points.

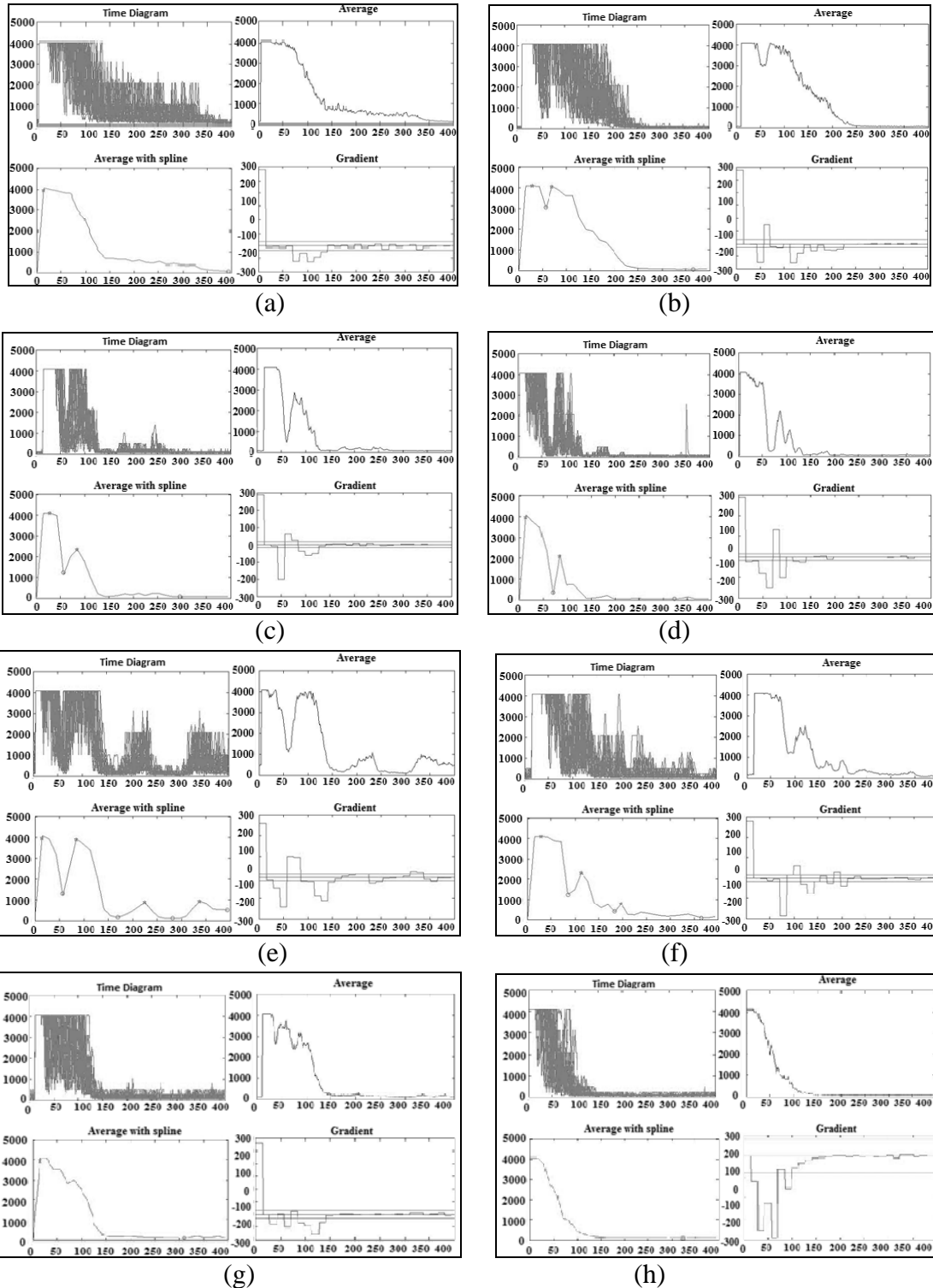


Figure 7: Time diagrams for eight classes (a) IFC, (b) IT, (c) IL1, (d) IL2, (e) ILM, (f) IEW, (g) IS, and (h) TP.

4.4 Calculation of peaks and valleys using gradient. The gradient has been calculated from the smoothed plot of the average diagram. The calculation of gradient has been done in a linear manner by dividing the difference of alternate data points of the interpolated function by the difference of the abscissa points. The peak and valley points of the curves are determined by setting a threshold over the curve of the gradient. For all the data classes a positive threshold value of +16 and a negative threshold value of -16 are set. The main logic for the determination of peaks and valleys is that as the gradient curve is gradually traced along the abscissa when the curve starting from a point below the negative threshold crosses the zero position and then extends over the positive threshold, then the point on the smoothed average plot corresponding to this point on the gradient plot is marked as a peak. Similarly for locating a valley, it is found that points starting from above the positive threshold and abruptly falling below the negative threshold correspond to the valleys, which are also similarly marked. The number of peaks and valleys information acquired from the different data sets. Figure 7 shows time diagram which represents average plot, spline as well as gradient for each data classes in support of entire description.

4.5 Calculation of Envelope Peak and Notch.

Envelope Peak (*enpk*): The peak property considers the number of peaks of the smoothed average time diagram. Here we have considered the number of peaks of the smooth envelope of the time diagram. Here also the sliding procedure has been applied.

Notch: Another property in the average time diagram is a notch before the first peak in some data classes. That is at first the plot remains at a very low value then suddenly rises. This is the case for IL1 class, whereas for others the diagram starts with a high value (e.g. IL2). We simply checked the average value at a low abscissa (say at 10). With this property it is possible to distinguish IL1 and IL2, both having 2 peaks and two valleys as shown in Fig. 8 for class IL1 and IL2.

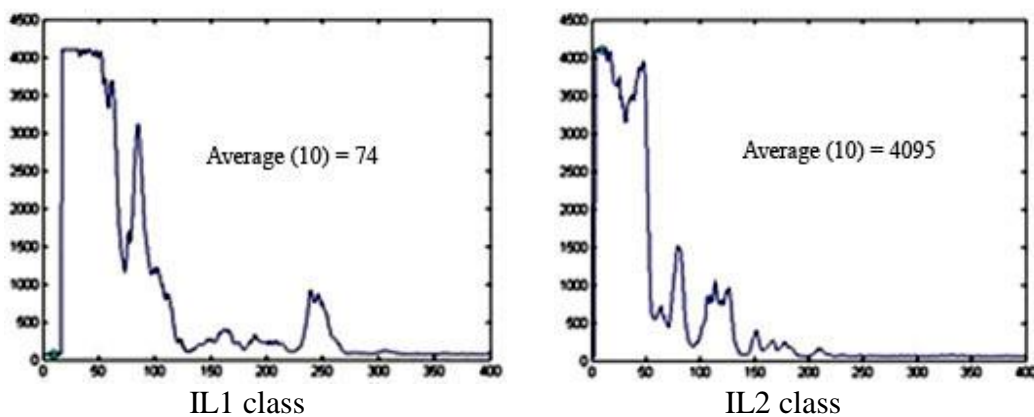


Figure 8: Peak and valley on average with spline curve

4.6 Calculation of Envelope Area, Integral1 and Integral2.

Envelope Area (*area*): This property considers the total area under the smooth envelope of the time diagram. This is calculated by trapezoidal method.

Integral1 (*int1*) and Integral2 (*int2*): These two properties are helpful to determine the width of the first peak of the smoothed average time diagram. For this, two equal intervals on the time axis of the time diagram, each of duration 120 points (i.e., from 1 to 120 and from 121 to 240) are considered. Then the fractional areas under the curve (the smooth averaged time diagram) are calculated in those two intervals. Now for a wide peak it's found that integral1 (area in the first interval) is around 0.7, i.e., around 70% of the total area and integral2 (area in the second interval) is around 0.25, i.e., around 25%. This is the case for classes having a wide peak (like IT) or classes having multiple peaks distributed throughout the time axis of the time diagram (like ILM, IEW) or classes having a single peak which is flat (IFC). Whereas for classes having a single narrow peak (IS) or having two peaks that are situated near the origin of the time axis (IL1 and IL2) the value of integral1 is higher, around 0.9 (i.e., around 90% of total area under the time diagram) and value of integral2 is much lower; around 0.09 (i.e., 9% of the total area). Values of integral1 (*int1*) and integral2 (*int2*) are calculated for each class.

4.7 Formation of Histograms. Histograms are plotted from the image intensity (range 0 to 255) of each class. Then frequency or number of occurrence for each intensity value is calculated and then normalised so that the frequency values lie within 0 and 1. Then these normalised frequencies are plotted in the form of bar diagram as shown in Fig. 9.

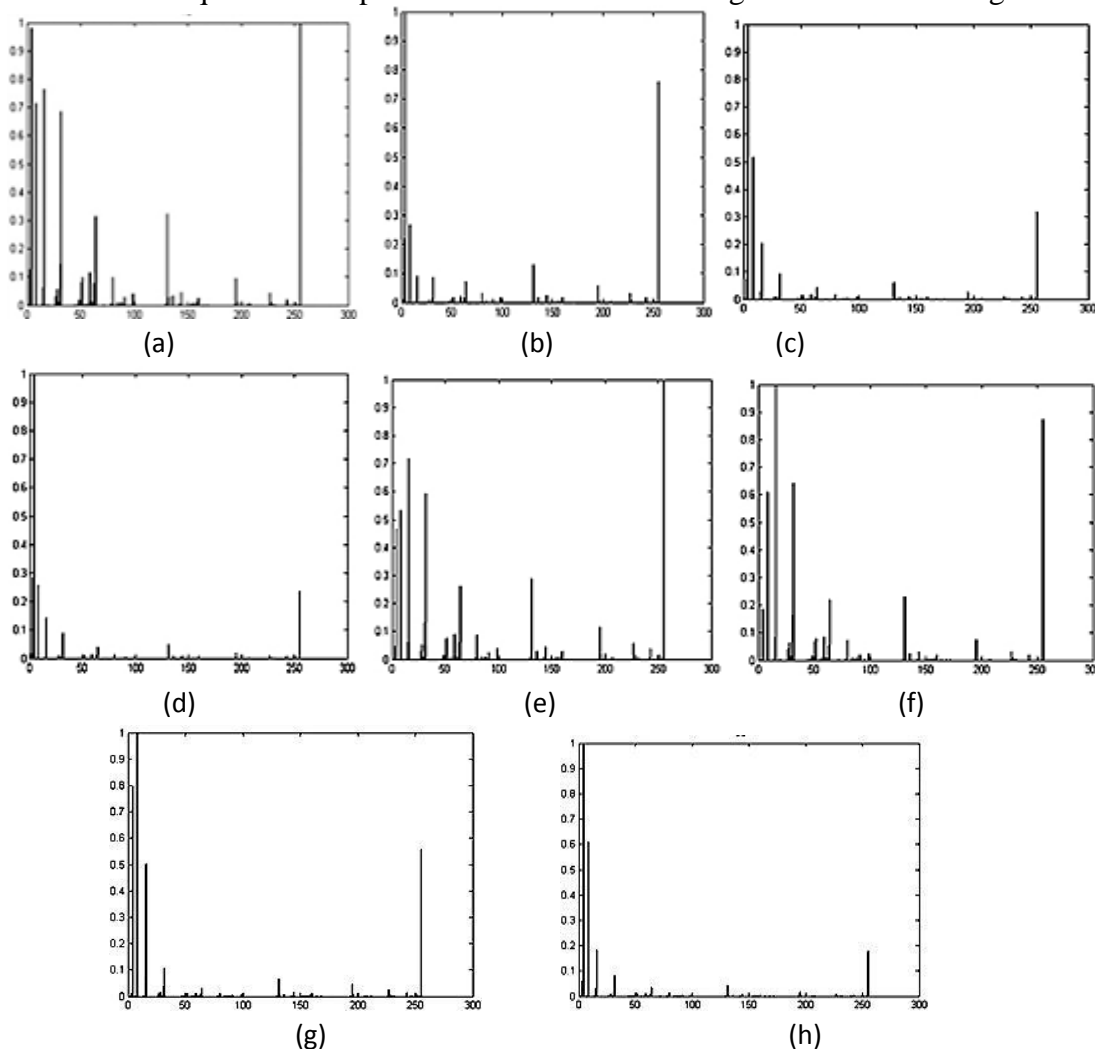


Figure 9: Histogram of different classes (a) IFC, (b) IT, (c) IL1, (d) IL2, (e) ILM, (f) IEW, (g) IS, and (h) TP.

4.8 Calculation of moments. Time diagram is constructed from the overall data. A mean of the several time diagrams of a single set of data is next formulated. After that smoothing of the mean time diagram is done in the form of spline. A scrutiny of the gradient curve devised from the smoothed mean permits to find out the peaks and valleys prevailing in the timing diagram. Further histograms are created for the individual data sets which provides further information to train the computer to categorize the data sets. The overall information fed into a properly devised neural network to design the model for the SODAR data classification to distinguish different thermal conditions existing in the atmosphere. For better classification another feature moment property extracted from the histogram of the data set. In the histogram, the moment of a pixel value or intensity about a pixel value 'a' is defined as the product of the normalized frequency of the corresponding intensity and its distance from the pixel value 'a'. For instance the moment of pixel value 50 about pixel value 'a' is $(50 - a) \times \text{freq}(50)$, where $\text{freq}(50)$ is the normalized frequency, i.e., ratio of frequency at pixel value 50 to the maximum frequency. 'a' can be designated as origin. Now root of the sum of squares of all the moment value is called the moment of a pixel value, which can be expressed by the expression

$$\sqrt{\sum (\text{frq}(i) \times (i - a))^2}, \text{ where, } 0 \leq i \leq 255.$$

This expression indicates the moment of the histogram about the pixel value 'a'. This moment is depicting the distribution of high frequencies values in the histogram. If all the pixels have equal frequency then their frequency will be same and equal to one. Then the corresponding histogram will have highest moment value, where as if the pixels near the origin (a) have very high frequency and pixels away from the origin have low frequency, then the moment of the corresponding histogram is very low. Thus by choosing proper origin we can find the distribution of frequencies along the pixel values. Three characteristic properties (features) *mom1*, *mom2*, and *mom3* are calculated from the histogram using the relation $\sqrt{(\text{frq}(i) \times (i - a))^2}$

where, $0 \leq i \leq 255$ and 'a' is a pixel value selected as the origin. Thus by choosing proper origin we can find the distribution of frequencies along the pixel values. These three are moments *mom1*, *mom2* and *mom3* are discussed below.

Moment1 or *mom1*: By observation it is revealed that better results can be obtained if moments are calculated around a value near origin (3 or 4). The first moment is calculated around the pixel value 4. Moment of the histograms with origin 'a' = 4, neglecting none of the pixel values.

Thus the moment1 is given as $\text{mom1} = \sqrt{(\text{frq}(i) \times (i - 4))^2}$.

Property *mom1*: for 15 set of data of each class are shown in the Table 3

Moment2 or *mom2*: Moment of the histograms with origin 'a' = 255, neglecting the pixel value 4. This moment is calculated around the pixel value 255. The frequency at pixel 4 (where the frequency is maximum for most of the cases) is also not considered in the calculation. The moment is given by the formula:

$$\text{mom2} = \sqrt{(\text{frq}(i) \times (i - 255))^2}$$

where, $\text{frq}(i)$ is the normalised frequency of *i*-th pixel, where $0 \leq i \leq 255$ & $i \neq 4$. However if the value of $\text{frq}(i)$ is very low, i.e., $\text{frq}(i) < 0.1$ then $\text{frq}(i)$ is set to 0.

Property *mom2*: for 15 set of data of each class are shown in the Table 4.

Table 3: Properties of *mom1* calculated from 15 data sets for each class

Dataset	IFC	IT	IL1	IL2	ILM	IEW	IS	TP
1	200.627	187.1682	253.171	57.303	253.2971	251.1372	147.797	2.1873
2	181.9152	187.5192	236.069	72.3605	254.4288	251.1388	137.3852	2.1406
3	212.6666	205.0207	254.4861	73.9646	252.382	251.03	158.8864	1.8505
4	253.8311	221.2805	254.6783	73.6677	252.3153	252.3113	143.3309	1.7793
5	254.605	205.2562	253.0337	70.9728	254.2145	253.7515	137.2602	2.5154
6	236.6449	190.8994	251.444	71.5256	255.228	252.5582	153.7046	53.9906
7	255.2277	183.9757	252.8994	85.2503	255.3426	251.015	134.9069	2.1693
8	229.6747	195.7422	254.8501	92.5031	254.961	251.2877	174.5302	2.2378
9	256.8657	176.204	251.8587	80.6994	255.2786	252.8044	130.1177	53.99
10	254.4648	170.8328	253.6656	83.3804	255.7131	228.1985	118.4336	1.931
11	255.2276	189.3008	254.6451	83.4151	254.2339	254.2976	145.388	3.013
12	253.8408	179.164	255.0891	87.1289	255.8725	158.8664	114.7713	55.1444
13	237.3543	185.4862	255.1799	83.9154	256.3313	137.7672	135.6846	52.3753
14	254.1546	191.3491	256.799	90.1087	255.8508	145.8815	95.2287	66.6693
15	251.9891	192.5122	232.5609	94.6438	255.7497	145.9685	113.6127	65.9072
Range	182 - 257	171 - 221	232 - 256	57 - 94	252 - 256	137 - 254	95 - 159	1.8 - 67

Table 4: Properties of *mom2* calculated from 15 data sets for each class

Dataset	IFC	IT	IL1	IL2	ILM	IEW	IS	TP
1	188.7569	87.1261	296.9469	148.4184	272.9416	222.7958	281.7648	135.0646
2	127.5579	103.1107	326.5689	119.4098	279.3822	223.698	267.0637	132.184
3	208.99	74.5837	248.2096	122.5426	283.8652	172.801	283.4711	114.2678
4	273.6995	103.3282	310.0982	112.1476	298.8288	182.4343	273.4535	109.8724
5	290.4878	99.1891	284.2479	110.4015	287.1984	225.4868	223.8192	155.3274
6	196.8338	67.327	246.1457	123.1892	292.4867	218.3203	266.2934	116.2702
7	191.1551	79.7913	241.9491	126.4405	257.9043	169.5943	266.1704	133.9537
8	243.4249	83.6711	307.6582	125.6575	277.0027	248.7162	314.5736	138.1835
9	254.5623	76.6452	259.7935	125.1006	260.2925	259.6073	264.8554	137.5589
10	232.5556	97.6545	243.7822	144.9138	257.4418	197.7819	263.3741	119.2414
11	242.5478	95.669	310.2965	135.0275	228.8214	308.8634	271.4879	186.0519
12	215.3991	68.1082	315.8189	143.4041	212.2447	185.3569	223.0354	106.5288
13	218.1794	64.4727	299.0734	158.516	247.2406	191.1066	275.4922	131.487
14	273.0989	86.2966	330.5897	172.8111	251.6459	195.84	231.0088	117
15	302.6373	89.359	354.5304	168.5485	237.3094	242.3318	343.0767	145.1469
Range	127-303	64-103	241-355	110-172	212-299	172-309	223-343	106-186

Moment3 or *mom3*: Moment of the histograms with origin ' a ' = 4, Neglecting the pixel value 255. This moment is calculated from the following formula:

$$mom3 = \sqrt{(frq(i) \times (i - 4))^2}$$

where, $frq(i)$ is the normalised frequency of i -th pixel value, $0 \leq i \leq 254$. In this case we have not considered the frequency of the pixel value 255. This eliminates the effect of the high frequency value of pixel 255 and gives more insight about the histogram pattern.

Property *mom3* : for 15 set of data of each class are shown in the Table 5.

Table 5: Properties of *mom3* calculated from 15 data sets for each class.

Dataset	IFC	IT	IL1	IL2	ILM	IEW	IS	TP
1	38.5314	1.4109	33.0842	3.9493	34.0357	8.3013	7.8957	2.1873
2	27.8528	1.0811	41.82	1.9338	41.6295	8.3486	6.4808	2.1406
3	34.8538	0.296	41.9782	1.9845	26.3753	3.8792	8.0482	1.8505
4	37.8054	0.9122	43.1284	1.8162	25.7294	25.6903	7.121	1.7793
5	42.6933	1.0033	32.0168	1.7879	40.2987	37.2671	5.3793	2.5154
6	58.9926	0.2672	14.9355	1.995	46.2639	28.0116	6.4004	1.8829
7	46.2622	0.9369	30.9371	2.0476	46.8919	2.7465	6.3875	2.1693
8	53.9751	0.9948	44.1316	2.0349	44.7672	12.022	10.5671	2.2378
9	54.5801	1.2412	20.7798	2.0259	46.542	30.1508	6.2482	2.2277
10	41.8491	1.5814	36.6776	2.3468	48.869	38.1635	6.0883	1.931
11	46.2614	1.5493	42.9318	3.1785	40.421	40.82	6.9288	3.013
12	37.87	1.103	45.491	3.875	49.6966	11.6909	4.8208	1.7252
13	37.4317	1.0441	45.9974	7.0993	52.0069	12.8478	7.3164	2.1293
14	39.9193	0.9526	54.2654	4.9652	49.5845	12.0714	5.7615	1.8947
15	22.3049	0.9637	56.8007	4.6754	49.06	11.5149	13.801	2.3506
Range	22 - 59	0.9 - 1.6	14 - 57	1.8 - 4.9	25 - 52	3.8 - 38	4.8 - 13.8	1.7 - 2.5

5. Design of Classifier Using Neural Network Multi-Layer Perceptron (MLP)

Multi-Layer Perceptron (MLP) neural network for the classification of SODAR structure using nine features (such as *peak*, *enpk*, *notch*, *area*, *int1*, *int2*, *mom1*, *mom2*, and *mom3*) is discussed in section 5.1. The system accepts digitized backscattered signal from file and select 4 minute data block. Nine different features are extracted from each data block using the method as discussed in section 4. Total 600 such data sets are considered for this classification work. For example, 10 such sets of extracted features for different classes are shown in Table 6. For the classification of SODAR structure, we can use the procedure as stated in Fig.10.

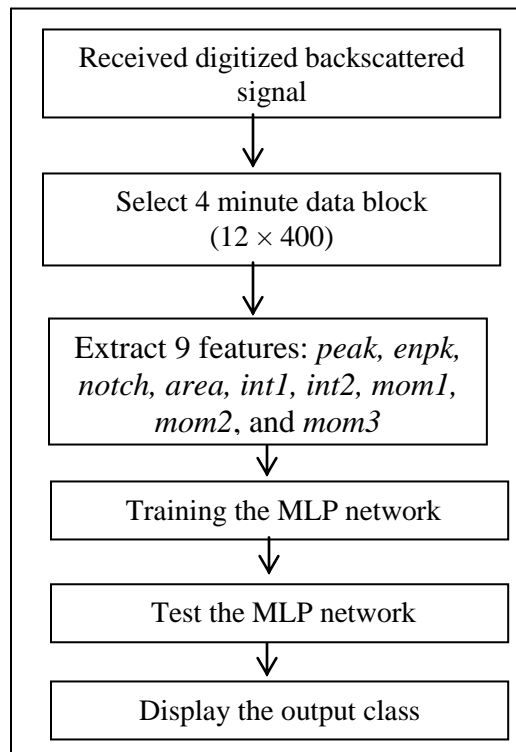


Figure 10: Classification flow diagrams

5.1 Neural Network Structure. We use a multi-layer perceptron (MLP) neural network to solve this problem. It consists of three or more layers of neurons of which the first layer is known as the input layer and the last one is known as output layer; remaining layers are called hidden layers. Figure 11 depicts the typical MLP network. The nodes in successive layers are fully connected but there is no connection within a layer. Every node, in the hidden layers and the output layer, computes the weighted sum of its input and applies a sigmoidal activation function to compute its output, which is then transmitted to the nodes of the next layers as input (Haykin, 1994). Objective of the MLP learning is to set the connection weights in such a way that the error between the network output and the target output is minimized. Back-propagation learning method is used to update the weights during learning the network. In this present network classifier design for the recognition of SODAR structure pattern has a layer of input, a hidden layer, and an output layer having 9, 9, and 8 nodes respectively. Nine computed features such as *peak*, *enpk*, *notch*, *area*, *int1*, *int2*, *mom1*, *mom2*, and *mom3* are used to design the neural network. So the number of input nodes for this MLP is nine. Also we have considered eight different classes of SODAR structures and the number of output nodes in the output layer is 8.

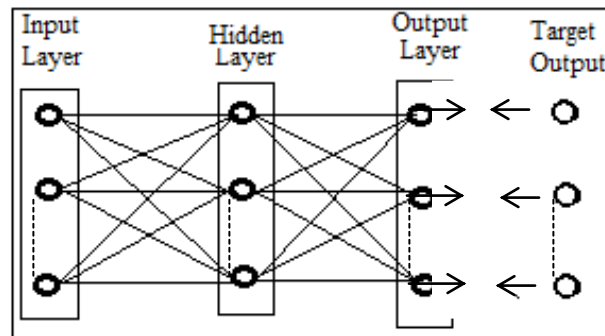


Figure 11: MLP neural networks for SODAR structure classification.

Input features have been computed from the selected data set and such 10 set of features for different class are tabulated in Table 6.

Table 6: Ten set of extracted features for different classes.

set	peak	enpk	notch	area	int1	int2	mom1	mom2	mom3
1	1	3	4095	847541	0.73	0.21	200.63	188.76	38.53
2	1	3	4095	820797	0.75	0.23	181.92	127.56	27.85
3	2	3	83.91	407379	0.85	0.08	57.30	148.42	3.95
4	3	4	67.25	475472	0.83	0.09	94.64	168.55	4.67
5	1	2	72.75	448617	0.89	0.05	83.38	144.91	2.35
6	2	3	67.33	456840	0.92	0.04	73.67	112.15	1.82
7	2	3	85.5	442470	0.92	0.04	70.97	110.40	1.79
8	3	5	4095	8.27E+05	0.68	0.18	254.22	287.19	40.29
9	2	4	67.67	4.52E+05	0.90	0.05	85.25	126.44	2.05
10	1	3	89.67	480000	0.90	0.04	92.50	125.66	2.03

We have prepared the data file with $9 + 8 = 17$ fields in a record of which 9 computed features as input and remaining 8 fields are output which indicate either presence by '1' or absence by '0'. That means in a record one of these eight output fields is one and remaining are zeros. These eight classes are defined in Table 7

Table 7: The arrangement of various classes in the output string

1	2	3	4	5	6	7	8
IFC	IT	IL1	IL2	ILM	IEW	IS	TP

5.2 Training and Test the Network. Initially, we mix the data set randomly. Then we partitioned the data into two parts, one part contains 80% of data used as training the model and the remaining 20% of these data used as test the performance of the trained model. This neural network (MLP) is trained with different hidden nodes such as 5, 6, 7, 8, 9, 10, 15, 20, 25, 30 up-to different levels of iterations from 300 to 1200. The performance of the model is tabulated in Tables 8 and 9.

Table 8: Percentage recognition score with training data set for different hidden node

No. of Iteration	For different hidden node (H)									
	H = 5	H = 6	H = 7	H = 8	H = 9	H = 10	H = 15	H = 20	H = 25	H = 30
300	73.778	82.667	84.444	89.556	88.667	86.444	92.444	93.778	94.222	93.333
400	74.444	81.333	86.667	86.889	90.667	89.111	94.667	97.778	92.889	94.000
500	76.222	84.222	84.667	88.000	89.556	92.000	96.444	95.111	96.667	95.111
600	79.778	82.889	86.667	90.000	91.111	91.556	96.889	96.222	98.222	96.889
700	74.000	82.889	86.000	88.222	91.333	91.333	96.667	97.111	96.444	96.667
800	78.889	85.556	85.778	90.889	90.444	91.556	94.889	98.000	95.556	97.111
900	78.667	82.222	87.333	88.889	92.444	91.556	96.000	97.556	97.778	98.222
1000	77.778	84.667	90.000	90.222	93.556	92.889	97.333	96.222	98.000	98.444
1100	75.778	83.778	87.556	90.222	90.667	92.000	96.222	98.667	97.556	98.000
1200	76.889	84.667	87.556	88.444	91.111	93.556	96.222	99.111	98.667	98.222

Table 9: Percentage recognition score with test data set for different hidden node

No. of Iteration	For different hidden node (H)									
	5	6	7	8	9	10	15	20	25	30
300	70.667	77.333	76.667	76.667	79.333	84.000	86.667	90.810	88.000	88.000
400	70.000	73.333	78.000	82.667	84.000	84.667	88.667	87.333	89.333	88.000
500	70.667	77.333	78.667	79.333	82.000	84.000	86.667	88.667	88.667	90.000
600	74.667	76.667	81.333	80.000	86.000	84.000	83.333	84.667	89.333	86.000
700	70.000	78.000	77.333	77.333	83.333	87.333	88.000	91.333	87.333	89.333
800	70.667	76.667	80.667	76.000	86.000	83.333	86.000	88.000	88.000	88.000
900	72.667	72.000	78.667	80.000	86.000	83.333	87.333	85.333	90.000	89.333
1000	71.333	80.667	81.333	80.667	87.333	87.333	85.333	89.333	90.667	91.333
1100	69.333	79.333	77.333	83.333	84.000	87.333	89.333	88.667	90.000	89.333
1200	72.000	79.333	78.667	83.333	84.000	82.000	85.333	90.000	88.000	90.000

6. Results and Conclusions

The neural network model (MLP) is designed for identification of atmospheric structures generated by a SODAR system using the knowledge, experiences and expertise of the

human expert working in this field. Table 8 and Table 9 depict the result of the performance of the present model of atmospheric structure classification. All eight classes are correctly classified in terms of accuracy. The Table 8 shows that 97.1% recognition score achieved for training set data, when model runs for 700 iterations with 20 hidden nodes, and 91.33% recognition score achieved for test set data, when model runs for 700 iterations with 20 hidden nodes as indicated in Table 9. Thus we have achieved successful classification of SODAR data.

The SODAR system has emerged as a useful remote sensing tool that provides information about the formation of different types of thermal structures like temperature inversion, thermal plumes, elevated multilayered inversion, fog layers, and other various types of PBL (Planetary Boundary Layer) structures, at low cost and continuous basis. It was evident that SODAR signatures were representing various structures believed to be associated with the formation and changes in the PBL characteristics. We designed classifier in the soft-computing paradigm can automatically recognize the PBL structures in order to avoid the tedious job of manual identification of the different types of useful SODAR patterns. We have used neural network architecture to classify eight different types of SODAR patterns and this may be one of the solutions of the SODAR pattern classification problems. Multi-layer perceptron (MLP) neural network models are inherently suitable in data-rich environments and extract underlying relationships from the data domain. The classifier reduces dependence on human experts for the identification of SODAR structure patterns. The results obtained by testing the model are satisfactory. This classifier tool may be applicable for both offline and online SODAR structure recognition. With this enhancement, we can develop a new SODAR system incorporating automatic structure classification scheme for different applications. Finally, this study holds promise for researchers working in the domains of atmospheric sciences, remote sensing, air pollution, meteorology, and civil aviation.

REFERENCES

1. Mcallister, L.G., Pollard, J.R.,Mahohey, A.R. & Shaw, P.J.R., (1969), Acoustic sounding – a new approach to the study of atmospheric structure. *Proceedings of IEEE*, v. 57, pp. 579–587.
2. Cronenwett, W.T., Walker, G.B. & Inman, R.L., (1972), Acoustic sounding of meteorological phenomena in the planetary boundary layer. *Journal of Applied Meteorology*, v. 11, pp. 1351–1358.
3. Beran, D.W., Hooke, W.H. & Clifford, S.F., (1973), Acoustic echo-sounding techniques and their application to gravity wave, turbulence and stability studies. *Earth and Environmental Science*, v. 4, pp. 133–153.

4. Frisch, A.S., & Clifford, S.F., (1974), A study of convection capped by a stable layer using Doppler radar and acoustic echo sounder, *Journal of Applied Meteorology*, v. 31, pp. 1622–1628.
5. Wendler, G., Kodama, Y., & Poggi, A., (1983), Katabatic winds in Adelie Land, *Antarctic Journal of United States*, v. 18, pp. 236- 238.
6. Asimakopoulous, D.N., Cole, R.S., Caughey, S.J. & Crease, B. A., (1976), A quantitative comparison between acoustic sounder returns and the direct measurement of atmospheric temperature fluctuations. *Boundary Layer Meteorology*, v. 10, pp. 137–148.
7. Deb, N. C., Naithani, J., & Kapoor, M., (1995), Design and Development of a PC controlled Acoustic Sounding System for Antarctica, Eleventh Indian Expedition to Antarctica, Scientific Report, Department of Ocean Development, Technical Publication No.9, pp. 79-86.
8. Deb, N.C., Pal, S., Patranabis, D. C., & Dutta, H. N., (2010), A neurocomputing model for sodar structure classification, *International Journal of Remote Sensing*, v. 31, 2995 – 3018.
9. Deb, N.C., Ray, K. S., & Dutta, H. N., (2011), SODAR Pattern Classification by Graph Matching, *IEEE Geosciences and Remote Sensing Letters*, v. 8, pp 483-487.
10. Kalogiros, J.A., Helmis, C.G., Asimakopoulos, D.N., Papageorgas, P.G. & Soilemes, A.T., (1995), A layer detection and classification algorithm for sodar facsimile records. *International Journal of Remote Sensing*, v. 16, pp. 2939–2954.
11. Mukherjee, A., Pal, P. & Das, J., (2002), Classification of sodar data using fractal features. Poster presentation at Proceedings of Indian Conference on Computer Vision, Graphics & Image Processing, 16–18 December, Ahmedabad, India, pp. 203-207.
12. Choudhury, S. & Mitra, S., (2004), A connectionist approach to SODAR pattern classification. *IEEE Geosciences and Remote Sensing Letters*, v. 1, pp. 42–46.
13. Chaudhuri, B.B., De, A.K., Gnaguly A. & Das, J., (1992), Automatic recognition and Interpretation of sodar records. *Indian Journal of Radio Space Physics*, v. 21, pp. 123–128.
14. Mukherjee, A., Pal, P. & Das, J., (1999), Identification of elementary sodar patterns using perceptrons. In Proceedings of fourth International Conference on advance in pattern recognition and digital techniques, December 1999, India. (New Delhi, India:Narosa) pp. 83-86.
15. Koul, P. N., (1995), A Report on the Operations Carried Out By Survey of India Team During Eleventh Indian Expedition to Antarctica; Eleventh Indian Expedition to Antarctica, Scientific Report, Department of Ocean Development, Technical Publication No.9, pp. 145-151.

16. Naithani, J., Dutta, H. N., Pasricha, P. K., Reddy, B. M., & Aggarwal, K. M., (1994), Evaluation of heat and momentum fluxes over Maitri, Antarctica, *Boundary Layer meteorology*, v. 74, pp.195-208.
17. Naithani, J., & Dutta, H. N., (1995), Acoustic sounder measurements of the planetary boundary layer at Maitri, Antarctica, *Boundary layer Meteorology*, v. 76, pp. 199-207.
18. Deb, N. C., Srivastava, M. K., Singh, R., Pasricha, P. K., & Dutta, H. N., (1999), Warm spell over Schirmacher region of east Antarctica during February, 1996, *DOD Tech Pub No. 13*, pp. 71-78.
19. Deb, N. C., Chowdhury, S., & Pal, A., (2001), Acoustic Remote Sensing of LPBL over Antarctica,” *Indian Journal of Physics*, v. 75B, pp. 259-262.
20. Dutta, H. N., Srivastava, M. K., Pasricha, P. K., Gajananda, Kh., Naithani, J., Deb, N. C., Ojha, D., & Gupta, V. B., (1999), Cyclone induced warming over a wide spread region in east Antarctica : a case study, *NPL Report No. DOD/12-MMDP/8-97-MRC Cell/01*, NPL, New Delhi, October, pp. 1-15.
21. Gajananda, Kh., Kaushik, A., & Dutta, H. N., (2004), Thermal convection over east Antarctica: Potential microorganism dispersal, *International Journal of Aerobiologia* v. 20, pp. 21-34.
22. Kumar, A., Gupta, V. B., Dutta, H. N., & Ghude, S., (2007), Mathematical modelling of katabatic winds over Schirmacher region, East Antarctica, *Indian J Radio & Space Phys.*, v. 36, pp. 204-212.
23. Haykin, S., (1994), *Neural Networks: A Comprehensive Foundation*, New York: Macmillan.